Sensors & Actuators: B. Chemical 379 (2023) 133228

Contents lists available at ScienceDirect

Sensors and Actuators: B. Chemical

journal homepage: www.elsevier.com/locate/snb

Biocompatible ratiometric fluorescent chemosensor for ultrasensitive detection of endogenous aminopeptidase N *In Vitro* and *In Vivo*

Mo Ma [a,b], Dianfeng Dai [a], Pinyi Ma [a,*], Qiong Wu [c], Dejiang Gao [a], Daqian Song [a,*]

[a] College of Chemistry, Jilin Province Research Center for Engineering and Technology of Spectral Analytical Instruments, Jilin University, Qianjin Street 2699, Changchun 130012, China
[b] School of Pharmacy, Jilin University, Qianjin Street 2699, Changchun 130012, China
[c] Nanomedicine and Translational Research Center, China-Japan Union Hospital of Jilin University, Changchun 130033, China

ARTICLE INFO

Keywords:
Aminopeptidase N (APN)
Fluorescent chemosensor
Nile blue (NB) derivative
Drug-induced liver injury (DILI)
Fluorescence imaging

ABSTRACT

Aminopeptidase N (APN) plays an important role in promoting the circulation of amino acids and influences many important physiological functions of organisms. Monitoring of APN level is of great value for the early clinical diagnosis and prognosis of diseases and certain cancers. In this study, we designed a ratiometric APN fluorescent chemosensor NB-APN by using Nile blue derivative as a fluorophore and alanyl as a recognition unit. After APN was recognized by alanyl of NB-APN, the NB previously blocked by the alanyl group was released, causing the inverse evolution trend of fluorescence intensitis of signal peaks at 675 nm and 610 nm. The ratiometric signal sensitively responded to the concentration of APN, and the detection limit was as low as 15 pg/mL. This chemosensor was successfuly applied for quantitative detection of APN in urine samples. Moreover, the chemosensor realized ratiometric fluorescence imaging of APN in *in vitro* and *in vivo*, and demonstrated the potential value of APN in the diagnosis and treatment of liver diseases in a drug-induced liver injury model. Therefore, the proposed chemosensor can potentially be applied in diagnosis of APN-related diseases.

1. Introduction

Aminopeptidase N (APN, EC 3.4.11.2), also known as alanine aminopeptidase or CD13, is a zinc ion-dependent exopeptidase that can hydrolyze neutral or basic amino acids at the N-terminus of a protein polypeptide chain to activate a series of important *in vivo* biochemical reactions [1,2]. APN is widely present in mammals and exists as a homodimer in cell membrane, and it has a variety of important physiological functions in human body [3,4]. When other urinary proteins are at normal levels, the presence of APN in urine indicates an early renal injury. Therefore, APN acts as an early biomarker of glomerulonephritis [5,6]. Drug-induced liver injury (DILI) is recognized as a major cause of acute liver injury [7–9]. The abnormal expression of several enzymes, such as aminopeptidases and oxidoreductases, may be a harbinger of DILI [10–12]. Additionally, APN is also a promising cancer biomarker since it exhibits enhanced enzyme activity in cancer cells [13–16]. Thus, the development of real-time detection methods of APN with high sensitivity and selectivity will promote diagnosis and pathophysiological study of APN-related diseases.

Due to its advantages of simplicity and convenience, non-invasiveness, real-time detection ability, high sensitivity, high spatio-temporal resolution, and applicability in *in vivo* imaging, fluorescence spectrometry has attracted much attention [17–23]. At present, fluorescent chemosensors for determining APN are mainly divided into two categories: affinity chemosensor [24–31] and reactive fluorescent chemosensor [32–42]. Although affinity fluorescent chemosensor can be used for fluorescence imaging of cancer cells or tumor transplanted nude mice, the interference from its background signals seriously affects the imaging quality. Large changes in fluorescent intensity or ratio of reactive fluorescent chemosensor before and after interacting with APN can effectively reduce the interference of background signals. Therefore, developing APN fluorescent chemosensor has gained increasing attention in recent years.

Nile Blue (NB) is a typical phenoxazine dye, which possesses well stability due to the rigid structure [43]. As a natural singly positively charged fluorophore, NB also exhibits good biocompatibility. With the rapid development of fluorescent chemosensor technology in the field of biology, NB has quickly become a hot spot of the current research owing to its excellent photophysical properties and chemical modifiability [44–48].

* Corresponding authors.
E-mail addresses: mapinyi@jlu.edu.cn (P. Ma), songdq@jlu.edu.cn (D. Song).

https://doi.org/10.1016/j.snb.2022.133228
Received 26 October 2022; Received in revised form 3 December 2022; Accepted 21 December 2022
Available online 24 December 2022

In this work, we designed and synthesized a long-wavelength ratiometric APN fluorescent chemosensor NB-APN using NB derivative as a fluorophore and alanyl as a recognition unit. The chemosensor showed a fluorescence emission peak at 610 nm, which is an obvious blue-shift peak compared with the peak of NB at 675 nm. The fluorophore NB was released as a result of the recognition and the hydrolysis of the alanyl group by APN, leading to obvious changes in the ratio of fluorescent signals. In the detection of APN in physiologically relevant environment, NB-APN exhibited unprecedented sensitivity, photostability, and fast responsiveness. The binding mode of NB-APN with APN and the corresponding reaction mechanism were investigated by molecular docking simulation and mass spectroscopy. The proposed chemosensor was successfully applied in quantitative detection of APN in 500-fold diluted urine, ratiometric fluorescence imaging of APN in normal hepatocytes and hepatoma cells and monitoring paracetamol (APAP)-induced hepatotoxicity *in vitro*. Further, this sensor was demonstrated to be capable of *in vivo* fluorescence imaging of APN in a mouse tumor and a drug-induced liver injury (DILI) model, indicating it a promising tool for clinical diagnosis of kidney and liver diseases.

2. Materials and methods

2.1. Organic Synthesis

The synthetic route of NB-APN was shown in Scheme 1. The reactants and instruments used in the synthesis process were provided in Supporting Information (SI). Compounds **1**, **2** and **NB** were synthesized based on previously reported methods (details can be found in SI). HR-MS, ^{1}H NMR, and ^{13}C NMR spectra of the compound were exhibited in Fig. S1–6.

First, Boc-L-alanine (0.1 mmol) and HATU (0.1 mmol) were dissolved in 5 mL of dichloromethane. Next, 40 μL of DIPEA was added, and the mixture was incubated in an ice bath for 30 min. After that, dichloromethane solution containing 0.12 mmol **NB** was added dropwise to the mixture, and the obtained dispersion was allowed to react at room temperature for 24 h before being separated by column chromatography (dichloromethane:methanol, 100:1). The resultant intermediate product was dissolved in dichloromethane, and 0.2 mL of CF_3COOH was added under vigorous stirring and kept for 3 h at room temperature. Sample purification was divided into two steps: removal of solvent by reduced pressure distillation and separation of solid by column chromatography (dichloromethane:methanol, 20:1), and the product **NB-APN** with a yield of 42% was obtained.

HR-MS (*m/z*) for $C_{27}H_{29}N_4O_6^+$ [NB-APN–ClO_4]$^+$: calculated, 505.2082; found: 505.2085. ^{1}H NMR (300 MHz, Methanol-d_4) δ 9.08 (d, 1 H), 8.62 (s, 1 H), 8.46 (d, J = 8.3 Hz, 1 H), 8.08 (d, J = 9.9 Hz, 1 H), 8.03 – 7.82 (m, 3 H), 7.33 (d, J = 2.5 Hz, 1 H), 4.52 (t, J = 7.0 Hz, 1 H), 3.99 (t, 4 H), 3.78 (s, 6 H), 2.60 (t, J = 7.1 Hz, 4 H), 1.77 (d, J = 7.1 Hz, 3 H). ^{13}C NMR (75 MHz, Methanol-d_4) δ 172.44, 171.58, 160.28, 151.83, 147.33, 144.64, 143.37, 136.76, 132.22, 132.06, 131.72, 130.03, 126.01, 124.84, 124.79, 123.94, 108.70, 98.38, 51.53, 51.48, 45.48, 29.98, 17.95.

2.2. Detection of APN in solution

A stock solution of NB-APN (1 mM) was prepared in DMSO. Four milliliters of PBS (10 mM, pH 7.4) and 50 μL of the NB-APN stock solution were vigorously mixed in a 5 mL centrifuge tube. After APN solution was added, the volume was adjusted to 5 mL with PBS. The reaction solution was shaken on a shaker at 37 °C for 20 min, and the fluorescence emission spectrum (λ_{ex} = 560 nm) and the absorption spectrum of the reaction were measured. The spectra of samples in the control group (without the addition of APN solution) were also collected under the same conditions. To assess the specificity of NB-APN toward APN, NB-APN was incubated with APN in the presence of other compounds/molecules commonly found in cells, including inorganic salts, bioactive molecules, reactive oxygen species, and aminopeptidase.

2.3. Detection of APN in urine samples

To evaluate its reliability, the NB-APN was employed to measure the recovery rates of APN in spiked human urine samples. First, fresh human urine was centrifuged (5000 rpm), and 1 mL of the urine was then mixed with 0.5, 0.75, or 1 μg of APN. Then, the mixture was diluted 500 times with PBS, and NB-APN (10 μM) was added into it and incubated for 20 min. Finally, the fluorescence intensity ratio (I_{675}/I_{610}) was measured by a fluorescence spectrometer. For comparison, APN in human urine samples were also detected using a commercial ELISA kit.

2.4. Detection of APN in vitro

The details of cell culture and cytotoxicity experiments were provided in SI. The cells were washed with PBS (10 mM, three times) before imaging. All cell imaging was carried out at an excitation wavelength of 559 nm, emission wavelengths of 580–620 nm (yellow channel) and 660–700 nm (red channel); and the images were collected through a 100 × 1.4 NA objective lens. Statistical analysis of the light intensity in the region of interest was performed on Image-J software.

2.4.1. Imaging of endogenous APN in cells

HepG2 and LO2 cells were incubated with 5 μM NB-APN for different time periods (0, 10, 20, 30, 40, and 60 min) prior to fluorescence imaging. Meanwhile, another group of HepG2 and LO2 cells were treated with 100 μM bestatin for 1 h, followed by 5 μM NB-APN for another 30 min before subjecting to fluorescence imaging. In another control group, HepG2 cells were first stained with 5 μM Hoechst33342 (a

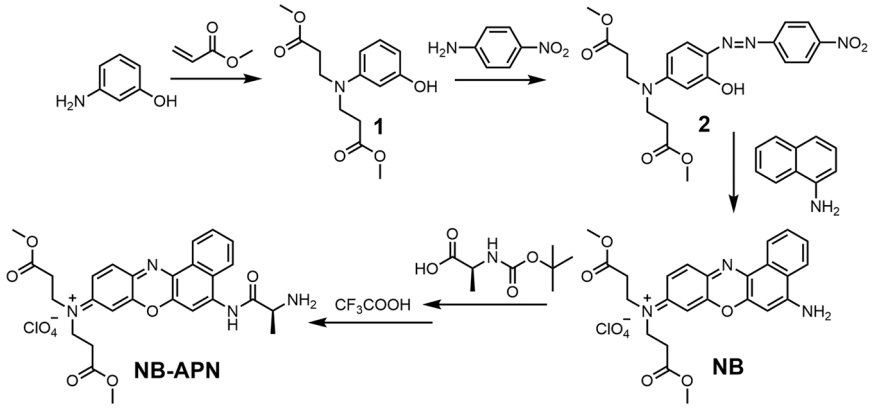

Scheme 1. Synthetic route of NB-APN.

nucleic acid dye) for 5 min, and the stained HepG2 cells were mixed with LO2 cells. The cell mixture was treated with 5 μM NB-APN for 30 min before being subjected to fluorescence imaging.

2.4.2. Exploration of relationship between APN, DILI and hepatoprotective agent in cells

In the first group, HepG2 cells were incubated with 5 μM NB-APN for 30 min. In the second and third groups, HepG2 cells were pretreated with different concentrations of APAP (acetaminophen, 500 or 1000 μM) for 12 h, followed by 5 μM NB-APN for 30 min. In the fourth to seventh groups, HepG2 cells were pretreated with different hepatoprotective agents (NAC (N-acetyl-*L*-cysteine), GSH (glutathione), or TIO (tiopronin), Glu (D-glucurone), each at 300 μM) for 1 h before incubating with 1000 μM APAP for 12 h, followed by 5 μM NB-APN for 30 min. All the seven groups of cells were subjected to fluorescence imaging thereafter.

2.5. Detection of APN in vivo

The procedures for establishing tumor models were provided in SI. *In vivo* imaging experiments were conducted by using a 560 nm excitation filter and a 680 nm emission filter.

2.5.1. In situ imaging

Mice were intratumorally pre-injected with PBS (50 μL) and bestatin (100 μM). After 1 h, 50 μM NB-APN (50 μL) was injected into the tumors of HepG2-induced tumor-bearing mice. The mice were anesthetized using isoflurane before performing fluorescence imaging at 0, 0.25, 0.5, 1.0, 2.0, or 4.0 h post-injection.

2.5.2. Imaging of DILI model

All mice were randomly divided into two groups (n = 3/group): 1) the control group (PBS), 2) mice intraperitoneal injected with APAP (300 mg/kg). After 6 h, all mice were then treated with 100 μL of NB-APN (200 μM) *via* intravenous injection. After anesthesia, the mice were subjected to fluorescent imaging at 12 h post-injection. Another drug-injected mice was sacrificed after being anesthetized with isoflurane, and the main organs (heart, liver, spleen, lung and kidney) were collected and then incubated with 200 μM NB-APN for 3 h before fluorescence imaging.

3. Results and discussion

3.1. Spectral characteristics and sensing mechanism

As shown in Fig. 1, the absorption and fluorescence spectra were significantly changed after NB-APN reacted with APN. On one hand, the maximum absorption peak at 600 nm was red-shifted to 620 nm. On the other hand, the fluorescence emission peak at 610 nm was red-shifted to 675 nm, resulting in an obvious change in the ratio of the fluorescent signals. Because of the reaction between NB-APN and APN, the ratio of the fluorescent signals (I_{675}/I_{610}) was increased by ~250 times, which indicates that the chemosensor is highly sensitive to APN. At the same time, the absorption and fluorescence spectra of the mixture were consistent with those of NB, revealing that the fluorophore NB was generated in the reaction system.

To further confirm the reaction mechanism, the solution was characterized by MS (Fig. S7). The characteristic mass of NB appeared at *m/z* 434.1712, which suggests that APN could specifically recognize the NB-APN and hydrolyze its alanyl group, leading to the release of the fluorophore NB. We also carried out theoretical calculations to investigate the luminous mechanism of NB-APN in the presence of APN. TDDFT calculations were used to analyze the optical properties based on the optimal excited state geometry (Fig. S8). The calculated HOMO–LUMO energy gap of the first vertical excited state of NB-APN and NB was 3.09 eV and 2.37 eV, respectively. The maximum emission peak for NB-APN was 630.10 nm (f =1.2587) and that for NB was 676.54 nm (f=1.1918), which corresponded to the red-shift in the fluorescence peak determined experimentally. Furthermore, the distance of charge transfer (D_{CT}) was detected based on the electron density variation and hole-electron theory [49,50]. The obtained D_{CT} value of NB-APN and NB was 3.439 Å and 1.281 Å, respectively. These results indicated that the fluorescence change was mediated mainly by intramolecular charge transfer (ICT). In addition, the molecular docking results revealed that NB-APN could form three hydrogen bonds with three amino acids (GLN206, SER410, and GLU413) in APN (Fig. S9). The binding energy between NB-APN and APN was calculated to be −8.88 kcal/mol, demonstrating that NB-APN has strong affinity for APN. Based on the above results, we proposed the recognition mechanism between NB-APN and APN (Scheme 2) as follows: APN specifically recognizes and digests the alanyl unit of NB-APN, resulting in the release of NB and the red-shift of fluorescence.

3.2. Optimization of reaction conditions

Effects of temperature, pH, and reaction time on the changes in fluorescence intensity ratios of the reaction were investigated in detail. As shown in Fig. S10, after NB-APN reacted with APN, the fluorescence ratio I_{675}/I_{610} increased rapidly and reached a plateau after 20 min. Throughout the detection process, the fluorescence of NB-APN was hardly affected, demonstrating that NB-APN has good photostability. At the same time, the fluorescence ratio of the reaction almost reached the maximum value under physiological conditions (37 °C, pH 7.4) at 20 min (Figs. S11 and S12). Considering the needs for subsequent cell imaging experiments, the physiological conditions (37 °C, pH 7.4) were employed as the reaction conditions and the reaction time was set as more than 20 min

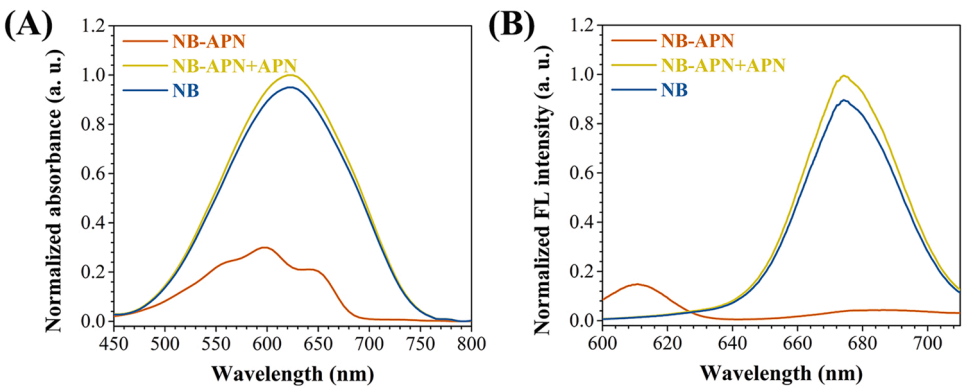

Fig. 1. (A) Absorption spectra and (B) fluorescence spectra of NB, NB-APN, and NB-APN in presence of APN (50 ng/mL) in PBS (10 mM, pH=7.4, 1% DMSO).

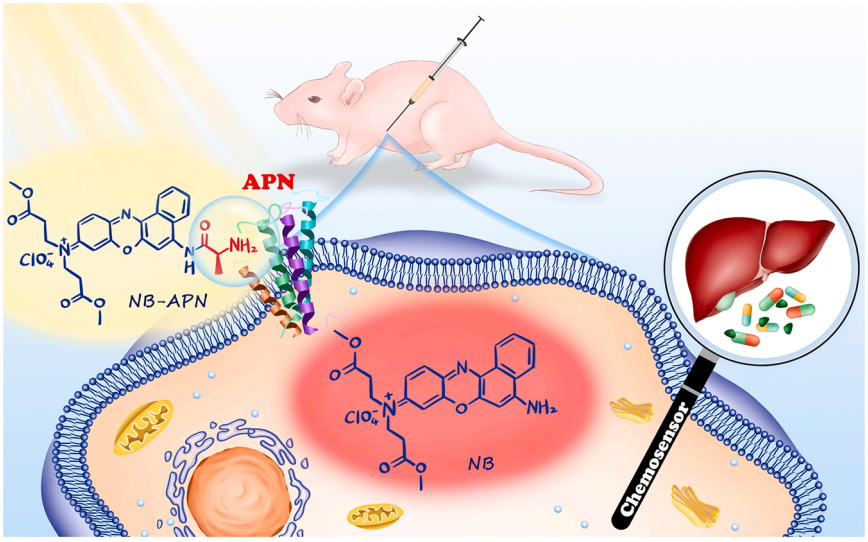

Scheme 2. Schematic illustration demonstrating the recognition mechanism between NB-APN (the chemosensor) and APN and its biological applications.

3.3. Analytical performance of NB-APN

Under the optimal experimental conditions, the fluorescence ratio I_{675}/I_{610} of NB-APN gradually increased with the APN concentration increasing from 0 to 50 ng/mL (Fig. 2A). The fitting result in Fig. 2B reveals that the fluorescence ratio I_{675}/I_{610} exhibited a linear relationship with the APN concentration from 0 to 10 ng/mL, which could be described as $I_{675}/I_{610} = 1.0742 \times [APN](ng/mL) + 0.2726$, $R^2 = 0.9962$. The limit of detection (LOD) of the developed chemosensor (calculated by 3σ/k) was 15 pg/mL, which is lower than those of previously reported methods (Table S1). Further, the kinetic of the enzymatic reaction was investigated according to Michaelis-Menten plot and Lineweaver-Burk plot. As shown in Fig. S13, $V_{max} = 23.58$ μM min^{-1}, $K_m = 0.21$ μM. The NB-APN have a good affinity to APN and is a highly sensitive and effective fluorescent substrate for APN.

As could be observed through inhibitor experiments (Fig. S14), bestatin [51], an inhibitor of APN, showed a significant inhibitory effect on the fluorescence signal ratio of the system, while exhibiting almost no influence on that of NB-APN and the fluorophore NB. This observation is a proof that the change in the fluorescence signal of the system is the result of the enzymatic activity of APN.

We investigated the reactivity of NB-APN towards some compounds and molecules commonly found in cells, including inorganic salts, bioactive molecules, reactive oxygen species, and enzymes. The result showed that fluorescence ratio I_{675}/I_{610} of the system increased significantly only in the presence of APN (Fig. S15), indicating that NB-APN has high selectivity toward APN. The observed selectivity could be mainly due to the specific recognition and the hydrolysis of alanyl groups by APN. Therefore, the developed NB-APN holds great potential to detect APN in complex biological systems.

3.4. Detection and visualization of APN in vitro

Glomerulonephritis is a major cause of advanced renal disease, and one of the most important indicators of the disease is the content of APN in urine [5,38]. Thus, developing rapid and sensitive method for detecting APN in urine is of great significance for the diagnosis of the disease. Therefore, we experimented NB-APN to detect APN in urine samples of healthy humans diluted by 500 times with PBS. Upon calculation, the content of APN in the urine samples of healthy humans was found to be 580 ng/mL, which was consistent with the test results obtained using commercial enzyme linked immunosorbent assay (ELISA) kits (Table S2). Moreover, APN at different concentrations was added to the urine samples to simulate the urine of patients with kidney disease, and the chemosensor and ELISA kits were used to detect APN in the samples. The results obtained from the two methods were not significantly different. Compared to the cumbersome operation of the ELISA kit, the detection of APN in urine samples by NB-APN is more simplified and timesaving.

The cytotoxicity of NB-APN was examined by the standard MTT

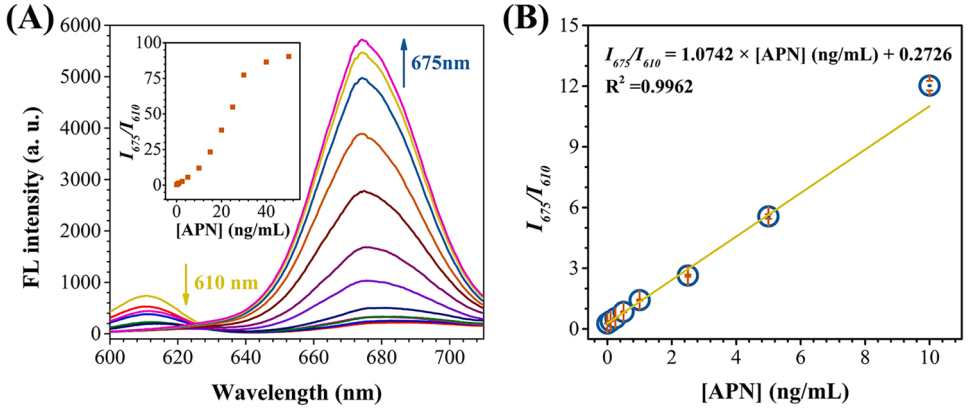

Fig. 2. (A) Fluorescence spectra of NB-APN (10 μM) in the presence of APN at various concentrations (0–50 ng/mL). (B) Variation of fluorescence intensity ratio (I_{675}/I_{610}) as a function of APN concentration. $\lambda_{em} = 560$ nm.

assay using HepG2 cells. As shown in Fig. S16, NB-APN showed negligible cytotoxicity in terms of cell viability even at a high concentration of 50 μM, suggesting the remarkable biocompatibility and feasibility for detecting APN in organisms.

The above *in vitro* studies and cell cytotoxicity experiments showed that NB-APN could detect APN with high sensitivity and selectivity, and it also had good biocompatibility and hypotoxicity. Therefore, we further applied the NB-APN in the imaging of APN in hepatoma cells HepG2 and normal hepatocytes LO2 [42]. As shown in Fig. 3, the fluorescence intensity in the red channel of HepG2 cells and LO2 cells incubated with the chemosensor gradually increased, causing the ratio R of the signals in red channel and yellow channel to gradually increase. The R-value reached a plateau at 30 min. Under the same conditions, the R value of HepG2 cells was significantly higher than that of LO2 cells, and the R values of both types of cells obviously decreased with the treatment of inhibitor bestatin. These results indicate that the change in the R values is the result of the enzymatic activity of APN, and the enzymatic activity of APN in HepG2 cells is prominently higher than that in LO2 cells. Moreover, HepG2 cells were co-cultured with LO2 cells and then incubated with 5 μM NB-APN, and the two cell lines could be easily distinguished through the fluorescence ratio (Fig. S17), which was also supported by the pre-staining of nucleus with Hoechst-33342. Further, we evaluated the activity of APN in A549, B16F10, HeLa, MG63 and HepG2 cells, and the obtianed results showed diverse levels of APN in different cell lines (Fig. S18), which was consistent with western blot analysis. Hence, the proposed NB-APN chemosensor could be considered as a promising tool for recognizing and determining intracellular APN through the high enzymatic activity of APN in liver cancer cells.

The overdose of antipyretic analgesic agent, APAP, has been reported to cause acute liver injury, and the concentration of aminopeptidase is increased during this process [12,52,53]. We assessed the performance of NB-APN in monitoring the changes of APN in APAP-induced acute hepatotoxicity and drug therapy (Fig. 4). First, we evaluated the production of APN in APAP-stimulated cells using NB-APN. HepG2 cells incubated with NB-APN exhibited obvious red fluorescence (R-value was greater than 4), proving the presence of intrinsic APN. When cells were pre-incubated with APAP for 12 h before being treated with NB-APN for 30 min, the R-value increased with the increase of APAP concentration. The increase of the R-value confirms the effectiveness of NB-APN in monitoring the changes of APN originated from APAP-induced hepatotoxicity. We further employed NB-APN to investigate the association of hepatotoxicity therapy and APN level in living cells. Four types of drugs (NAC, GSH, TIO, and Glu) were used as hepatoprotective agents against DILI [10]. The noticeable depression of red fluorescence was observed after the addition of the four drugs to HepG2 cells. Through the measurement of fluorescence intensity ratio, APN was used as a therapeutic indicator of hepatotoxicity, and the obtained results suggested that GSH as an antidote to APAP toxicity might be superior to NAC, Glu and TIO. The underlying mechanism was most likely due to the intake of GSH facilitating liver detoxification and reducing damage caused by APAP [54]. In addition, the results from western blotting and fluorescence imaging were also coincident with the above observations. All these findings indicated that NB-APN was highly sensitive to the fluctuation of intracellular APN after APAP stimulation and

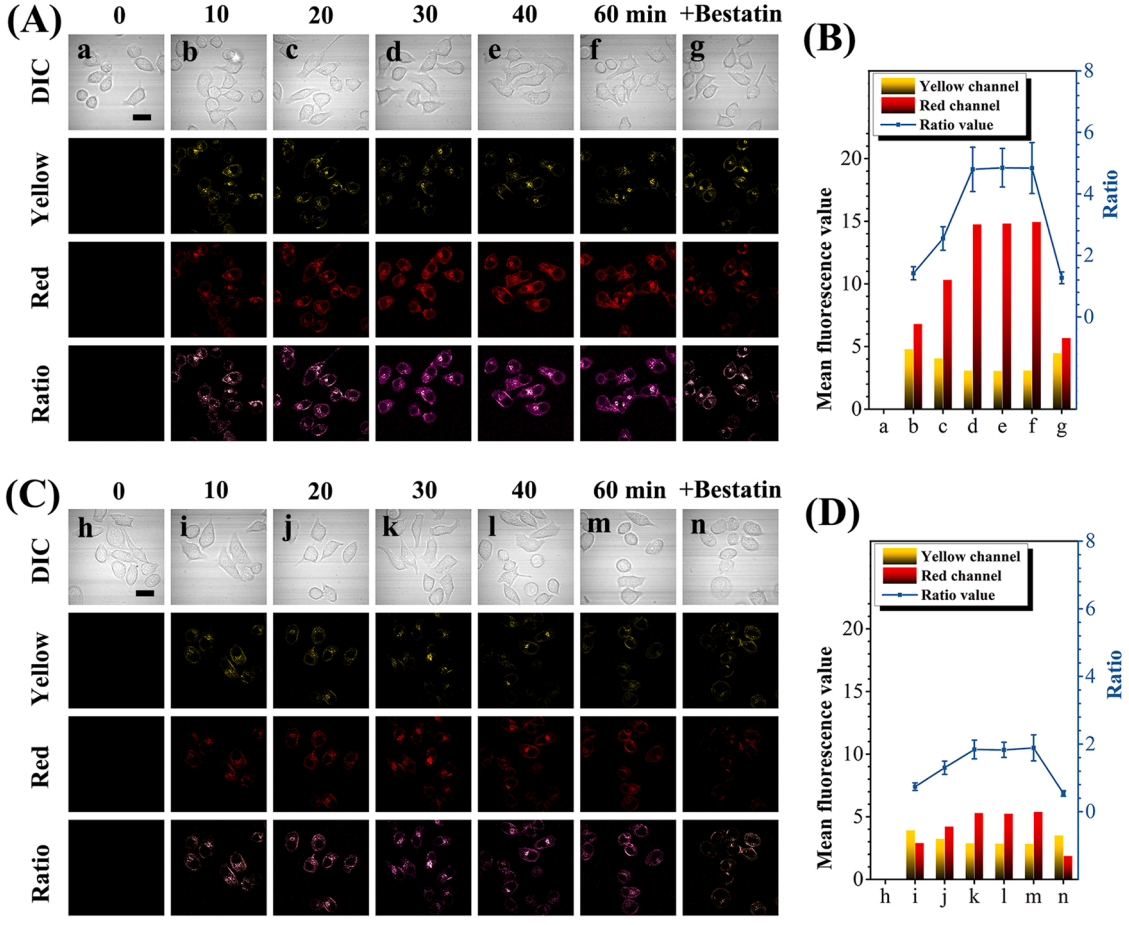

Fig. 3. Fluorescence images of (A) HepG2 cells and (C) LO2 cells incubated with NB-APN (10 μM) for different periods of time (0, 10, 20, 30, 40, and 60 min). Cells in column g in (A) and column n in (B) were treated with bestatin (100 μM) for 1 h, followed by NB-APN (5 μM) for 30 min. Scale bar = 20 μm. The corresponding mean fluorescence intensity in the yellow channel (580–620 nm) and the red channel (660–700 nm) and fluorescence ratios (I_{red}/I_{yellow}) of (A) are shown in (B), and those of (C) are shown in (D). λ_{ex} = 559 nm.

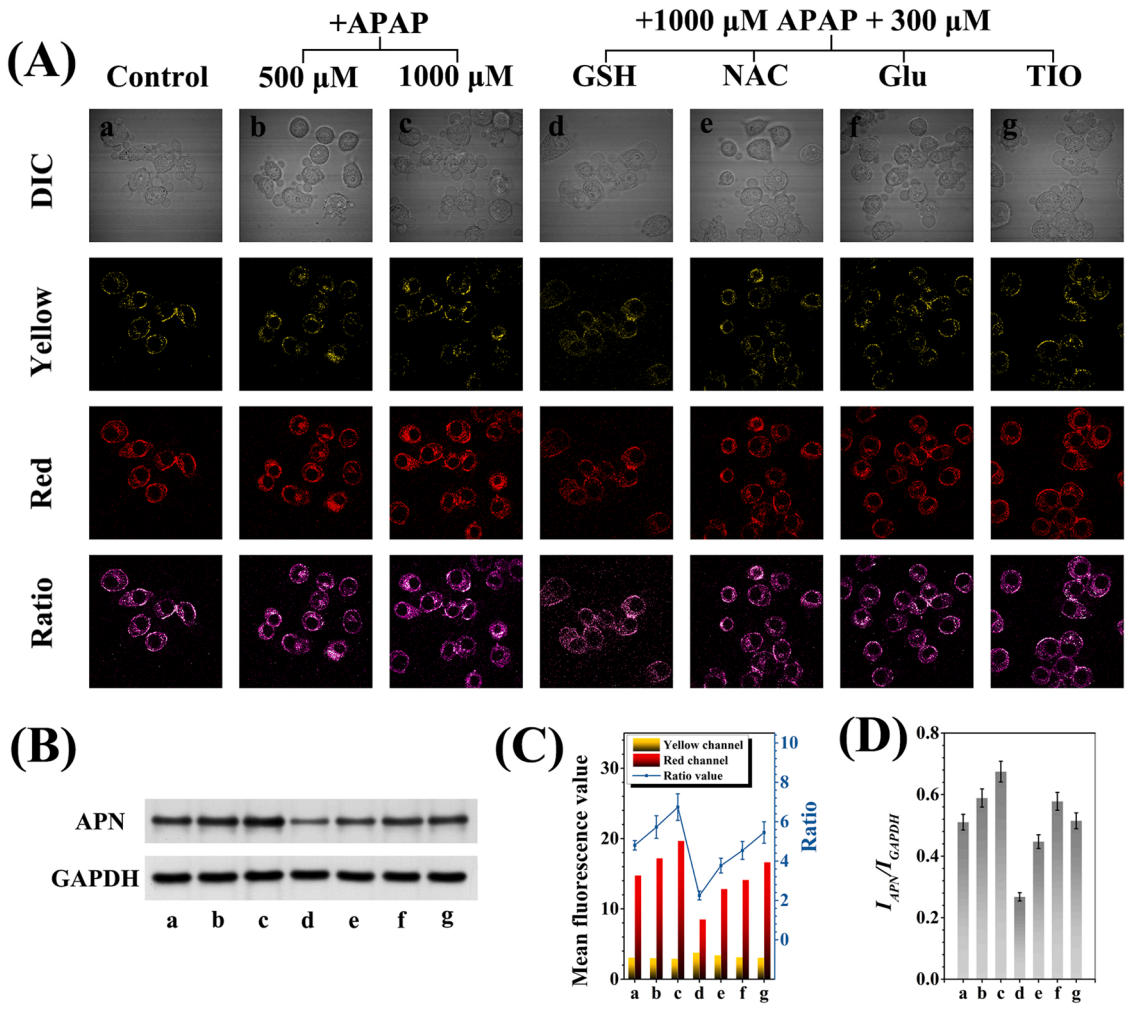

Fig. 4. Fluorescence images (A) and western blot analysis (B) of HepG2 cells incubated with APN in the presence of different compounds.(a) HepG2 cells + NB-APN (5 μM). (b-c) HepG2 cells + APAP (500 μM, b) or APAP (1000 μM, c) + NB-APN (5 μM). (d-g) HepG2 cells + NAC (d), GSH (e), Glu (f) or TIO (g) (each at 300 μM) + APAP (1000 μM) + NB-APN (5 μM). (C) The corresponding red fluorescence ratios (I_{red}/I_{yellow}) of (A). (D) The corresponding mean intensity ratio (I_{APN}/I_{GAPDH}) of (D). GAPDH was used as a protein standard.

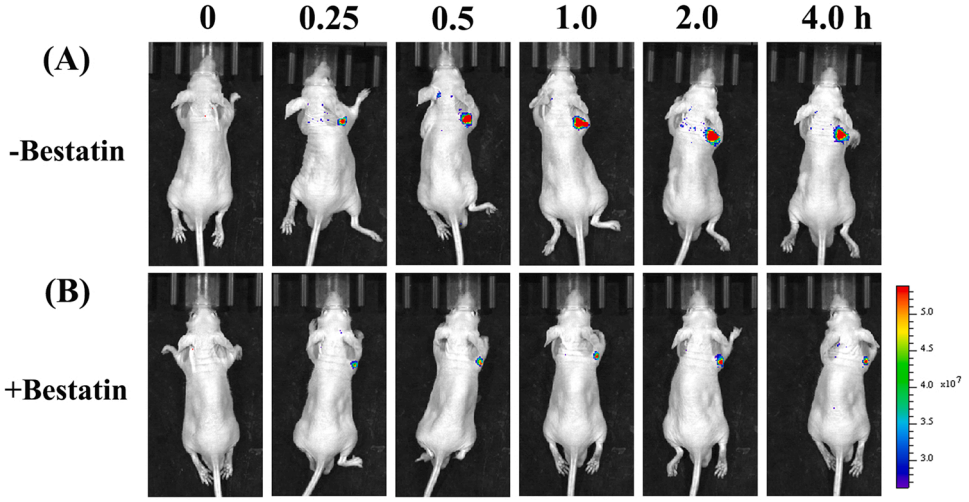

Fig. 5. *In situ* fluorescence images of HepG2 tumor-bearing mice. Mice were intratumorally injected with 50 μL of (A) PBS (control) and (B) bestatin (100 μM in PBS) for 1 h and then subjected to intratumoral injection with 50 μL of NB-APN (50 μM) in PBS for different periods of time (0, 0.25, 0.5, 1.0, 2.0, and 4.0 h).

could be used to evaluate the protective effect of drugs against DILI.

3.5. In vivo fluorescence imaging of APN

To evaluate the imaging performance of NB-APN *in vivo*, the chemosensor was further applied to image tumors in a liver tumor mouse model. To increase tissue penetration and eliminate autofluorescence, we employed the fluorescence in the red channel. As shown in Fig. 5, before the intratumoral injection with NB-APN, the background fluorescence signal of the mouse was very low. After NB-APN were intratumorally injected in mice of the experimental group, an obvious fluorescent signal appeared at the tumor site, and the signal could sustain for 4 h. In contrast, when mice in the control group were injected with a solution of the APN inhibitor bestatin, the fluorescence signal at the tumor site became significantly lower compared with that of mice in the experimental group. Therefore, it can be concluded that the fluorescence signal observed in the tumor site was caused by the enzyme activity of APN and NB-APN were capable of detecting APN *in vivo*.

Furthermore, we imaged the *in vivo* APN activity in DILI nude mice using NB-APN. As depicted in Fig. S19, the background fluorescence signal of mice with intraperitoneal injection of PBS and intravenous injection of NB-APN, was very low after 12 h post-injection. However, the fluorescence signal of the liver of nude mice intraperitoneally injected with 300 mg/kg APAP, followed by NB-APN, was strong after 12 h post-injection. This implies that APN was up-regulated in the DILI model. In addition, another drug-injected mice was sacrificed, and the main organs (heart, liver, spleen, lung and kidney) and tumors pretreated with NB-APN for 3 h were collected and subjected to imaging. As shown in Fig. S19C, the fluorescence signal only existed in liver. These results suggest that the chemosensor suits for biopsy of tumor tissue and has a significant clinical value.

4. Conclusions

In summary, we designed and synthesized an ultrasensitive ratiometric fluorescent chemosensor NB-APN for highly selective and sensitive detection of APN. Furthermore, it was successfully applied in the determination of APN in urine, as well as in the imaging of APN in cells and mouse tumor model. Preliminary results showed that the chemosensor could differentiate between liver tumor cells and normal cells, thus was successfully used to monitor the effectiveness of the remediation of APAP-induced hepatotoxicity. In the constructed mouse model of DILI, we observed an increase in the expression of APN in the liver, revealing the potential value of APN in the diagnosis and treatment of liver diseases. Taken together, this work presents a promoising APN detection method that can be utilized in clinical diagnosis.

CRediT authorship contribution statement

Mo Ma: Conceptualization, Investigation, Data curation, Validation, Writing – original draft. **Dianfeng Dai**: Formal analysis, Software, Data curation, Investigation. **Pinyi Ma:** Conceptualization, Project administration, Funding acquisition, Data curation, Writing – review & editing, Software. **Qiong Wu**: Investigation, Resources, Writing – review & editing. **Dejiang Gao:** Validation, Writing – review & editing. **Daqian Song:** Project administration, Funding acquisition, Resources, Supervision.

Declaration of Competing Interest

The authors declare that they have no known competing financial interests or personal relationships that could have appeared to influence the work reported in this paper.

Data Availability

Data will be made available on request.

Acknowledgments

This work was supported by the National Natural Science Foundation of China (22004046 and 22074052), the Norman Bethune Program of Jilin University (2022B21), the Natural Science Foundation of Jilin Province (YDZJ202101ZYTS024).

Appendix A. Supporting information

Supplementary data associated with this article can be found in the online version at doi:10.1016/j.snb.2022.133228.

References

[1] Y. Aozuka, K. Koizumi, Y. Saitoh, Y. Ueda, H. Sakurai, I. Saiki, Anti-tumor angiogenesis effect of aminopeptidase inhibitor bestatin against B16-BL6 melanoma cells orthotopically implanted into syngeneic mice, Cancer Lett. 216 (2004) 35–42.
[2] L. Chen, Y.-L. Lin, G. Peng, F. Li, Structural basis for multifunctional roles of mammalian aminopeptidase N, Proc. Natl. Acad. Sci. USA 109 (2012) 17966–17971.
[3] F.M. Barnieh, P.M. Loadman, R.A. Falconer, Is tumour-expressed aminopeptidase N (APN/CD13) structurally and functionally unique? Bba-Rev. Cancer 2021 (1876), 188641.
[4] S. Kumaravel, G.-R. Luo, S.-T. Huang, H.-Y. Lin, C.-M. Lin, Y.-C. Lee, Development of a novel latent electrochemical molecular substrate for the real-time monitoring of the tumor marker aminopeptidase N in live cells, whole blood and urine, Biosens. Bioelectron. 203 (2022), 114049-114049.
[5] B. Holdt-Lehmann, A. Lehmann, G. Korten, H.R. Nagel, H. Nizze, P. Schuff-Werner, Diagnostic value of urinary alanine aminopeptidase and N-acetyl-beta-D-glucosaminidase in comparison to alpha(1)-microglobulin as a marker in evaluating tubular dysfunction in glomerulonephritis patients, Clin. Chim. Acta 297 (2000) 93–102.
[6] C. Lu, M.A. Amin, D.A. Fox, CD13/Aminopeptidase N is a potential therapeutic target for inflammatory disorders, J. Immunol. 204 (2020) 3–11.
[7] S. Feng, J. Zheng, J. Zhang, Z. Gui, G. Feng, Fe^{2+} imaging in ferroptosis and drug-induced liver injury with a ratiometric near-infrared fluorescent probe, Sens. Actuators B Chem. 371 (2022), 132512.
[8] S. Feng, Z. Zheng, S. Gong, G. Feng, A unique probe enables labeling cell membrane and Golgi apparatus and tracking peroxynitrite in Golgi oxidative stress and drug-induced liver injury, Sens. Actuators B Chem. 361 (2022), 131751.
[9] Y. Deng, G. Feng, Visualization of ONOO$^-$ and viscosity in drug-induced hepatotoxicity with different fluorescence signals by a sensitive fluorescent probe, Anal. Chem. 92 (2020) 14667–14675.
[10] D. Cheng, J. Peng, Y. Lv, D. Su, D. Liu, M. Chen, et al., De novo design of chemical stability near-infrared molecular probes for high-fidelity hepatotoxicity evaluation in vivo, J. Am. Chem. Soc. 141 (2019) 6352–6361.
[11] D. Pessayre, A. Mansouri, A. Berson, B. Fromenty, Mitochondrial involvement in drug-induced liver injury, Handb. Exp. Pharmacol. (2010) 311–365.
[12] D. Cheng, W. Xu, X. Gong, L. Yuan, X.-B. Zhang, Design strategy of fluorescent probes for live drug-induced acute liver injury imaging, Acc. Chem. Res. 54 (2021) 403–415.
[13] P. Mina-Osorio, The moonlighting enzyme CD13: old and new functions to target, Trends Mol. Med. 14 (2008) 361–371.
[14] B. Bauvois, D. Dauzonne, Aminopeptidase-N/CD13 (EC 3.4.11.2) inhibitors: chemistry, biological evaluations, and therapeutic prospects, Med. Res. Rev. 26 (2006) 88–130.
[15] I. Saiki, H. Fujii, J. Yoneda, F. Abe, M. Nakajima, T. Tsuruo, et al., Role of aminopeptidase N (CD13) in tumor-cell invasion and extracellular matrix degradation, Int. J. Cancer 54 (1993) 137–143.
[16] M. Wickstrom, R. Larsson, P. Nygren, J. Gullbo, Aminopeptidase N (CD13) as a target for cancer chemotherapy, Cancer Sci. 102 (2011) 501–508.
[17] M.H. Lee, J.S. Kim, J.L. Sessler, Small molecule-based ratiometric fluorescence probes for cations, anions, and biomolecules, Chem. Soc. Rev. 44 (2015) 4185–4191.
[18] Y. Zhang, G. Zhang, Z. Zeng, K. Pu, Activatable molecular probes for fluorescence-guided surgery, endoscopy and tissue biopsy, Chem. Soc. Rev. 51 (2022) 566–593.
[19] C. Liu, X. Gao, J. Yuan, R. Zhang, Advances in the development of fluorescence probes for cell plasma membrane imaging, TRAC-Trend Anal. Chem. 133 (2020), 116092.
[20] H.-H. Han, H. Tian Jr., Y. Zang, A.C. Sedgwick, J. Li, J.L. Sessler, et al., Small-molecule fluorescence-based probes for interrogating major organ diseases, Chem. Soc. Rev. 50 (2021) 9391–9429.
[21] C. Li, G. Chen, Y. Zhang, F. Wu, Q. Wang, Advanced fluorescence imaging technology in the near-Infrared-II window for biomedical applications, J. Am. Chem. Soc. 142 (2020) 14789–14804.

[22] L. Jiang, T. Chen, E. Song, Y. Fan, D. Min, L. Zeng, et al., High-performance near-infrared fluorescence probe for fast and specific visualization of harmful sulfite in food, living cells, and zebrafish, Chem. Eng. J. 427 (2022), 131563.
[23] Y. Wen, Z. Long, X. Bai, F. Huo, C. Yin, Specific fluorescence release based on synergistic activation of enzymes and position-dependent of electrophilic groups to diagnose intrahepatic cholestasis of pregnancy, Chem. Eng. J. 440 (2022), 135978.
[24] H. Chen, H. Wang, X.-J. Qin, C. Chen, L. Feng, L.-Z. Chen, et al., A bestatin-based fluorescent probe for aminopeptidase N cell imaging, Chin. Chem. Lett. 26 (2015) 513–516.
[25] Y. Xi, D. Wang, T. Wang, L. Huang, X.-E. Zhang, Quantitative profiling of CD13 on single acute myeloid leukemia cells by super-resolution imaging and its implication in targeted drug susceptibility assessment, Nanoscale 11 (2019) 1737–1744.
[26] Z. Zhang, H. Harada, K. Tanabe, H. Hatta, M. Hiraoka, S. Nishimoto, Aminopeptidase N/CD13 targeting fluorescent probes: synthesis and application to tumor cell imaging, Peptides 26 (2005) 2182–2187.
[27] A. von Wallbrunn, J. Waldeck, C. Hoeltke, M. Zuehlsdorf, R. Mesters, W. Heindel, et al., In vivo optical imaging of CD13/APN-expression in tumor xenografts, J. Biomed. Opt. 13 (2008), 011007.
[28] A.H. Negussie, J.L. Miller, G. Reddy, S.K. Drake, B.J. Wood, M.R. Dreher, Synthesis and in vitro evaluation of cyclic NGR peptide targeted thermally sensitive liposome, J. Control Release 143 (2010) 265–273.
[29] Y. Tang, A. Shao, J. Cao, H. Li, Q. Li, M. Zeng, et al., cNGR-based synergistic-targeted NIR fluorescent probe for tracing and bioimaging of pancreatic ductal adenocarcinoma, Sci. China Chem. 61 (2018) 184–191.
[30] Y. Cheng, C. Sun, X. Ou, B. Liu, X. Lou, F. Xia, Dual-targeted peptide-conjugated multifunctional fluorescent probe with AIEgen for efficient nucleus-specific imaging and long-term tracing of cancer cells, Chem. Sci. 8 (2017) 4571–4578.
[31] Y. Saito, H. Yatabe, I. Tamura, Y. Kondo, R. Ishida, T. Seki, et al., Structure-guided design enables development of a hyperpolarized molecular probe for the detection of aminopeptidase N activity in vivo, Sci. Adv. 8 (2022) eabj2667.
[32] J. Li, L. Chen, W. Wu, W. Zhang, Z. Ma, Y. Cheng, et al., Discovery of bioluminogenic probes for aminopeptidase N imaging, Anal. Chem. 86 (2014) 2747–2751.
[33] X. He, Y. Hu, W. Shi, X. Li, H. Ma, Design, synthesis and application of a near-infrared fluorescent probe for in vivo imaging of aminopeptidase N, Chem. Commun. 53 (2017) 9438–9441.
[34] L. Varadi, E.Y. Najib, D.E. Hibbs, J.D. Perry, P.W. Groundwater, A selective, dual emission beta-alanine aminopeptidase activated fluorescent probe for the detection of pseudomonas aeruginosa, burkholderia cepacia, and serratia marcescens, Molecules 24 (2019) 3550.
[35] L. Feng, Z. Tian, M. Zhang, X. He, X. Tian, Z. Yu, et al., Real-time identification of gut microbiota with aminopeptidase N using an activable NIR fluorescent probe, Chin. Chem. Lett. 32 (2021) 3053–3056.
[36] U. Lee, T.-I. Kim, S. Jeon, Y. Luo, S. Cho, J. Bae, et al., Native chemical ligation-based fluorescent probes for cysteine and aminopeptidase N using meso-thioester-BODIPY, Chem. Eur. J. 27 (2021) 12545–12551.
[37] Y. Liu, C. Xu, H.-W. Liu, L. Teng, S. Huan, L. Yuan, et al., Precipitated fluorophore-based molecular probe for in situ imaging of aminopeptidase N in living cells and tumors, Anal. Chem. 93 (2021) 6463–6471.
[38] X. He, Y. Xu, W. Shi, H. Ma, Ultrasensitive detection of aminopeptidase N activity in urine and cells with a ratiometric fluorescence probe, Anal. Chem. 89 (2017) 3217–3221.
[39] L. Chen, W. Sun, W. Li, J. Li, L. Du, W. Xu, et al., The first ratiometric fluorescent probe for aminopeptidase N, Anal. Methods 4 (2012) 2661–2663.
[40] L. Chen, W. Sun, J. Li, Z. Liu, Z. Ma, W. Zhang, et al., The first ratiometric fluorescent probes for aminopeptidase N cell imaging, Org. Biomol. Chem. 11 (2013) 378–382.
[41] M. Xiao, W. Sun, J. Fan, J. Cao, Y. Li, K. Shao, et al., Aminopeptidase-N-activated theranostic prodrug for NIR tracking of local tumor chemotherapy, Adv. Funct. Mater. 28 (2018), 1805128.
[42] H. Li, Y. Li, Q. Yao, J. Fan, W. Sun, S. Long, et al., In situ imaging of aminopeptidase N activity in hepatocellular carcinoma: a migration model for tumour using an activatable two-photon NIR fluorescent probe, Chem. Sci. 10 (2019) 1619–1625.
[43] J. Jose, Y. Ueno, K. Burgess, Water-soluble nile blue derivatives: syntheses and photophysical properties, Chem. Eur. J. 15 (2009) 418–423.
[44] J. Fan, H. Dong, M. Hu, J. Wang, H. Zhang, H. Zhu, et al., Fluorescence imaging lysosomal changes during cell division and apoptosis observed using Nile Blue based near-infrared emission, Chem. Commun. 50 (2014) 882–884.
[45] J. Fan, S. Guo, S. Wang, Y. Kang, Q. Yao, J. Wang, et al., Lighting-up breast cancer cells by a near-infrared fluorescent probe based on KIAA1363 enzyme-targeting, Chem. Commun. 53 (2017) 4857–4860.
[46] B. Gurram, M. Li, J. Fan, J. Wang, X. Peng, Near-infrared fluorescent probe for fast track of cyclooxygenase-2 in Golgi apparatus in cancer cells, Front. Chem. Sci. Eng. 14 (2020) 41–52.
[47] B. Wang, J. Fan, X. Wang, H. Zhu, J. Wang, H. Mu, et al., A Nile blue based infrared fluorescent probe: imaging tumors that over-express cyclooxygenase-2, Chem. Commun. 51 (2015) 792–795.
[48] A. Ringaci, A.V. Yaremenko, K.G. Shevchenko, S.D. Zvereva, M.P. Nikitin, Metal-organic frameworks for simultaneous gene and small molecule delivery in vitro and in vivo, Chem. Eng. J. 418 (2021), 129386.
[49] Z. Liu, T. Lu, Q. Chen, An sp-hybridized all-carboatomic ring, cyclo 18 carbon: Electronic structure, electronic spectrum, and optical nonlinearity, Carbon 165 (2020) 461–467.
[50] T. Lu, F. Chen, Multiwfn: a multifunctional wavefunction analyzer, J. Comput. Chem. 33 (2012) 580–592.
[51] Y. Luan, J. Mu, W. Xu, The review of the synthesis of bestatin, an effective inhibitor of aminopeptidase N, Mini-Rev. Org. Chem. 5 (2008) 134–140.
[52] H.-W. Liu, L. Chen, C. Xu, Z. Li, H. Zhang, X.-B. Zhang, et al., Recent progresses in small-molecule enzymatic fluorescent probes for cancer imaging, Chem. Soc. Rev. 47 (2018) 7140–7180.
[53] J. Chen, D. Huang, M. She, Z. Wang, X. Chen, P. Liu, et al., Recent progress in fluorescent sensors for drug-induced liver injury assessment, ACS Sens. 6 (2021) 628–640.
[54] D. Han, M. Shinohara, M.D. Ybanez, B. Saberi, N. Kaplowitz, Signal transduction pathways involved in drug-induced liver injury, Handb. Exp. Pharmacol. (2010) 267–310.

Mo Ma is currently a PhD student in College of Chemistry, Jilin University. His interest is spectral analysis.

Dianfeng Dai is currently a PhD student in College of Chemistry, Jilin University. His interest is spectral analysis.

Pinyi Ma gained his doctor's degree from College of Chemistry, Jilin University in 2017 and he is an associate professor in that school. His research area is spectral analysis.

Qiong Wu gained her doctor's degree from College of Chemistry, Jilin University in 2018 and she is an associate professor in China-Japan Union Hospital of Jilin University. Her research area is spectral analysis and biosensor.

Dejiang Gao gained his doctor's degree from College of Chemistry, Jilin University in 2008 and he is a professor in that school. His research areas is spectral analysis.

Daqian Song gained his doctor's degree from College of Chemistry, Jilin University in 2003 and he is a professor in that school. His research areas are spectral and chromatography analysis.